The Astrophysical Journal, 595:1039–1051, 2003 October 1

WAVE EFFECTS IN THE GRAVITATIONAL LENSING OF GRAVITATIONAL WAVES FROM CHIRPING BINARIES

Ryuichi Takahashi and Takashi Nakamura
Department of Physics, Kyoto University, Kyoto 606-8502, Japan
Received 2003 February 13; accepted 2003 June 6

ABSTRACT

In the gravitational lensing of gravitational waves, wave optics should be used instead of geometrical optics when the wavelength λ of the gravitational waves is longer than the Schwarzschild radius of the lens mass M_L. For gravitational lensing of chirp signals from the coalescence of supermassive black holes at redshift $z_S \sim 1$ relative to the *Laser Interferometer Space Antenna*, the wave effects become important for a lens mass smaller than $\sim 10^8\ M_\odot$. For such cases, we compute how accurately we can extract the mass of the lens and the source position from the lensed signal. We consider two simple lens models: the point-mass lens and the SIS (singular isothermal sphere). We find that the lens mass and the source position can be determined to within $\sim 0.1\%$ of $[(\mathrm{S/N})/10^3]^{-1}$ for a lens mass larger than $10^8\ M_\odot$ and $\gtrsim 10\%$ of $[(\mathrm{S/N})/10^3]^{-1}$ for a lens mass smaller than $10^7\ M_\odot$ because of the diffraction effect, where S/N is the signal-to-noise ratio of the unlensed chirp signals. For the SIS model, if the source position is outside the Einstein radius, only a single image exists in the geometrical optics approximation, so that the lens parameters cannot be determined, while in the wave optics cases we find that the lens mass can be determined even for $M_L < 10^8\ M_\odot$. For the point-mass lens, one can extract the lens parameters even if the source position is far outside the Einstein radius. As a result, the lensing cross section is an order of magnitude larger than that for the usual strong lensing of light.

Subject headings: binaries: general — gravitational lensing — gravitational waves

1. INTRODUCTION

In-spirals and mergers of compact binaries are the most promising gravitational-wave sources and will be detected by ground-based as well as space-based detectors in the near future (e.g., Cutler & Thorne 2002). Laser interferometers are now coming on-line or are planned for broad frequency bands: for the high-frequency band 10–10^4 Hz, ground-based interferometers such as the Tokyo Advanced Medium-Scale Antenna (TAMA-300), the Laser Interferometer Gravitational-Wave Observatory (LIGO), Variability of Irradiance and Gravity Oscillations (VIRGO), and GEO-600 will be operated; for the low-frequency band 10^{-4} to 10^{-1} Hz, the *Laser Interferometer Space Antenna*[1] (*LISA*) will be in operation; for the intermediate-frequency band 10^{-2} to 1 Hz, space-based interferometers such as the *Decihertz Interferometer Gravitational Wave Observatory* (*DECIGO*; Seto, Kawamura, & Nakamura 2001) are planned. For the templates of the chirp signals from coalescing compact binaries, post-Newtonian computations of the waveforms have been done by many authors. Using the matched filter techniques with the template, we can obtain the binary parameters such as the mass and the spatial position of the source (e.g., Cutler & Flanagan 1994).

If the gravitational waves from a coalescing binary pass near massive objects, gravitational lensing should occur in the same way as it does for light. The gravitational lensing of light is usually treated in the geometrical optics approximation, which is valid in all observational situations (Schneider, Ehlers, & Falco 1992; Nakamura & Deguchi 1999). However, for the gravitational lensing of gravitational waves, the wavelength is long, so that the geometrical optics approximation is not valid in some cases. For example, the wavelength λ of the gravitational waves for the space interferometer is ~ 1 AU, which is extremely larger than that of visible light ($\lambda \sim 1\ \mu$m). As shown by several authors (Ohanian 1974; Bliokh & Minakov 1975; Bontz & Haugan 1981; Thorne 1983; Deguchi & Watson 1986a), if the wavelength λ is larger than the Schwarzschild radius of the lens mass M_L, the diffraction effect is important and the magnification is small. To see the reason why the ratio M_L/λ determines the significance of the diffraction, we consider a double slit with the slit width comparable to the Einstein radius $\xi_{\mathrm{E}} \sim (M_L D)^{1/2}$, where D is the distance from the screen to the slit (Nakamura 1998). When waves with wavelength λ pass through the slit, the interference pattern is produced on the screen. The width l of the central peak of the interference pattern is $l \sim (D/\xi_{\mathrm{E}})\lambda$. Then, the maximum magnification of the wave flux is of the order of $\sim \xi_{\mathrm{E}}/l \sim M_L/\lambda$. Thus, the diffraction effect is important for

$$M_L \lesssim 10^8\ M_\odot \left(\frac{f}{\mathrm{mHz}}\right)^{-1}, \qquad (1)$$

where f is the frequency of the gravitational waves. However, as suggested by Ruffa (1999), the region focused by the gravitational lensing would have a relatively large area because of the diffraction, so that the lensing probability would increase. Since the gravitational waves from compact binaries are coherent, interference is also important (Mandzhos 1981; Ohanian 1983; Schneider & Schmid-Burgk 1985; Deguchi & Watson 1986b; Peterson & Falk 1991). Thus, we expect wave effects (diffraction and interference) to provide much information about the lens objects.

In this paper we consider the wave effects in the gravitational lensing of gravitational waves. We take the

[1] See http://lisa.jpl.nasa.gov/index.html.

coalescence of supermassive black holes (SMBHs) of mass 10^4–10^7 $M_\odot$ as the sources. SMBH binaries are some of the most promising sources for *LISA* and will be detected with a very high signal-to-noise ratio, S/N $\sim 10^3$ (Bender et al. 2000). Since the merging SMBH events will be detected for extremely high redshift ($z > 5$), the lensing probability is relatively high, and hence some lensing events are expected. We consider two simple lens models: (1) a point-mass lens in which compact objects (such as black holes) are assumed as lens objects and (2) an SIS (singular isothermal sphere) lens in which galaxies, star clusters, and CDM (cold dark matter) halos are assumed as lenses. The wave effects become important for a lens mass of 10^6–10^9 $M_\odot$, which is determined by the *LISA* band, 10^{-4} to 10^{-1} Hz, from equation (1). The frequency of the gravitational waves from a coalescing SMBH binary chirps, so that we can see wave effects for different frequencies in the lensed chirp signals.

We calculate the gravitationally lensed waveform using wave optics for the two lens models: the point-mass lens and the SIS. Then, we investigate how accurately we can extract information on the lens object from the gravitationally lensed signals detected by *LISA* using the Fisher matrix formalism (e.g., Cutler & Flanagan 1994). Cutler (1998) studied the estimation errors for merging SMBHs by *LISA* (see also Vecchio & Cutler 1998; Hughes 2002; Moore & Hellings 2002; Hellings & Moore 2003; Seto 2002; Vecchio 2003). Following Cutler (1998), we calculate the estimation errors, especially for the lens mass and the source position. We assume a 1 yr observation before the final merging and consider a lens mass in the range 10^6–10^9 $M_\odot$. Then, the typical time delay between double images would be 10–10^4 s, which is much smaller than 1 yr.

This paper is organized as follows: In § 2 we briefly review the wave optics in gravitational lensing for the point-mass lens and the SIS model. In § 3 we discuss the gravitationally lensed waveforms detected with *LISA* and mention the parameter estimation based on the matched filtering analysis. In § 4 we numerically evaluate the S/N and the parameter estimation errors. We discuss the dependence of the estimation errors on the lens model, the lens mass, and the source position. In § 5 we estimate the lensing event rate. Section 6 is devoted to summary and discussions. We assume a $(\Omega_M,\ \Omega_\Lambda) = (0.3,\ 0.7)$ cosmology and a Hubble parameter $H_0 = 70$ km s^{-1} Mpc^{-1} and use units of $c = G = 1$.

2. WAVE OPTICS IN GRAVITATIONAL LENSING

In this section we briefly review the wave optics in the gravitational lensing of gravitational waves (Schneider et al. 1992; Nakamura & Deguchi 1999). We consider gravitational waves propagating under the gravitational potential of a lens object. The metric is given by

$$ds^2 = -(1+2U)\,dt^2 + (1-2U)\,d\boldsymbol{r}^2 \equiv g^{(B)}_{\mu\nu}\,dx^\mu\,dx^\nu\ , \quad (2)$$

where $U(\boldsymbol{r})$ ($\ll 1$) is the gravitational potential of the lens object. Let us consider the linear perturbation $h_{\mu\nu}$ in the background metric tensor $g^{(B)}_{\mu\nu}$ as

$$g_{\mu\nu} = g^{(B)}_{\mu\nu} + h_{\mu\nu}\ . \quad (3)$$

Under the transverse traceless Lorentz gauge condition of $h^\nu_{\mu;\nu} = 0$ and $h^\mu_\mu = 0$, we have

$$h^{;\alpha}_{\mu\nu;\alpha} + 2R^{(B)}_{\alpha\mu\beta\nu}h^{\alpha\beta} = 0\ , \quad (4)$$

where the semicolon denotes the covariant derivative with respect to $g^{(B)}_{\mu\nu}$ and $R^{(B)}_{\alpha\mu\beta\nu}$ is the background Riemann tensor. If the wavelength λ is much smaller than the typical radius of curvature of the background, we have

$$h^{;\alpha}_{\mu\nu;\alpha} = 0\ . \quad (5)$$

Following the eikonal approximation to the above equation by Baraldo, Hosoya, & Nakamura (1999), we express the gravitational wave as

$$h_{\mu\nu} = \phi e_{\mu\nu}\ , \quad (6)$$

where $e_{\mu\nu}$ is the polarization tensor of the gravitational wave ($e^\mu_\mu = 0,\ e_{\mu\nu}e^{\mu\nu} = 2$) and ϕ is a scalar. The polarization tensor $e_{\mu\nu}$ is parallel-transported along the null geodesic ($e_{\mu\nu;\alpha}k^\alpha = 0$, where k^α is a wavevector; Misner, Thorne, & Wheeler 1973). Then, the change of the polarization tensor by gravitational lensing is of the order of U ($\ll 1$), which is very small in our observational situation, and hence we can regard the polarization tensor as a constant. Thus, we treat the scalar wave ϕ, instead of the gravitational wave $h_{\mu\nu}$, propagating through the curved spacetime. The propagation equation of the scalar wave is

$$\partial_\mu\left(\sqrt{-g^{(B)}}\,g^{(B)\mu\nu}\,\partial_\nu\phi\right) = 0\ . \quad (7)$$

For the scalar wave in the frequency domain $\tilde{\phi}(f,\ \boldsymbol{r})$, the above equation (7) with equation (2) is rewritten as

$$\left(\nabla^2 + \omega^2\right)\tilde{\phi} = 4\omega^2 U\tilde{\phi}\ , \quad (8)$$

where $\omega = 2\pi f$. The above equation (8) can be solved by using the Kirchhoff integral theorem (Schneider et al. 1992).

It is convenient to define the amplification factor as

$$F(f) = \frac{\tilde{\phi}^L(f)}{\tilde{\phi}(f)}\ , \quad (9)$$

where $\tilde{\phi}^L(f)$ and $\tilde{\phi}(f)$ are the lensed and unlensed ($U = 0$ in eq. [8]) gravitational-wave amplitudes, respectively. In Figure 1 we show the gravitational lens geometry of the source, the lens, and the observer. Here, D_L, D_S, and D_{LS} are the distances to the lens, to the source, and from the source to the lens, respectively, and $\boldsymbol{\eta}$ is the position vector of the source in the source plane, while $\boldsymbol{\xi}$ is the impact parameter in the lens plane. We use the thin-lens approximation in which the lens is characterized by the surface mass density $\Sigma(\boldsymbol{\xi})$ and the gravitational waves are scattered on the thin-lens plane. Then, the amplification factor $F(f)$ at the observer is given by (Schneider et al. 1992)

$$F(f) = \frac{D_S\xi_0^2}{D_L D_{LS}}\,\frac{f}{i}\int d^2\boldsymbol{x}\,\exp[2\pi i f t_d(\boldsymbol{x},\ \boldsymbol{y})]\ , \quad (10)$$

where $\boldsymbol{x} = \boldsymbol{\xi}/\xi_0$, $\boldsymbol{y} = \boldsymbol{\eta}D_L/\xi_0 D_S$ is the source position, ξ_0 is the arbitrary normalization constant of the length, t_d is the arrival time at the observer from the source, and F is normalized such that $|F| = 1$ in the no-lens limit ($U = 0$).

Although we do not take account of cosmological expansion in the metric, equation (2), we can apply the

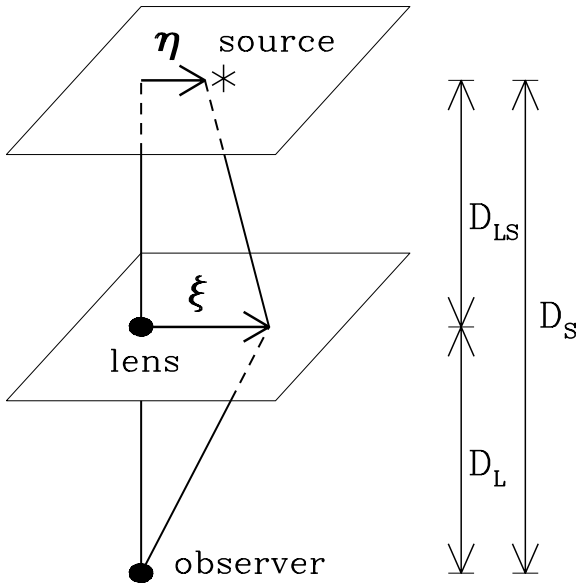

FIG. 1.—Gravitational lens geometry for the source, the lens, and the observer. Here D_L, D_S, and D_{LS} are the distances between them, $\boldsymbol{\eta}$ is the displacement of the source, and $\boldsymbol{\xi}$ is an impact parameter. We use the thin-lens approximation in which the gravitational waves are scattered in the thin-lens plane.

result without cosmological expansion to cosmological situations, since the wavelength of the gravitational waves is much smaller than the horizon scale. What we should do is (1) take the angular diameter distances and (2) replace f with $f(1+z_L)$, where z_L is the redshift of the lens (Baraldo et al. 1999). Then, the amplification factor $F(f)$ in equation (10) is rewritten in cosmological situations as

$$F(f)=\frac{D_S\xi_0^2(1+z_L)f}{D_LD_{LS}}\frac{f}{i}\int d^2\boldsymbol{x}\,\exp[2\pi i f t_d(\boldsymbol{x},\,\boldsymbol{y})]\,, \tag{11}$$

where D_L, D_S, and D_{LS} denote the angular diameter distances. The arrival time t_d at the observer from the source position $\boldsymbol{\eta}$ through $\boldsymbol{\xi}$ is given by (Schneider et al. 1992)

$$t_d(\boldsymbol{x},\,\boldsymbol{y})=\frac{D_S\xi_0^2}{D_LD_{LS}}(1+z_L)\left[\frac{1}{2}|\boldsymbol{x}-\boldsymbol{y}|^2-\psi(\boldsymbol{x})+\phi_m(\boldsymbol{y})\right]\,. \tag{12}$$

The nondimensional deflection potential $\psi(\boldsymbol{x})$ is determined by

$$\nabla_x^2\psi=\frac{2\Sigma}{\Sigma_{\rm cr}}\,, \tag{13}$$

where ∇_x^2 denotes the two-dimensional Laplacian with respect to $\boldsymbol{x}$, Σ is the surface mass density of the lens, and $\Sigma_{\rm cr}=D_S/(4\pi D_LD_{LS})$. We choose $\phi_m(\boldsymbol{y})$ so that the minimum value of the arrival time is 0. We derive $\psi(\boldsymbol{x})$ and $\phi_m(\boldsymbol{y})$ in the following subsections for the point-mass lens and the SIS model.

In the geometrical optics limit ($f\gg t_d^{-1}$), the stationary points of $t_d(\boldsymbol{x},\,\boldsymbol{y})$ contribute to the integral of equation (11) so that the image positions $\boldsymbol{x}_j$ are determined by the lens equation

$$\frac{\partial t_d(\boldsymbol{x},\,\boldsymbol{y})}{\partial\boldsymbol{x}}=0\,. \tag{14}$$

This is just Fermat's principle. The integral on the lens plane (in eq. [11]) is reduced to the sum over these images (Nakamura & Deguchi 1999):

$$F(f)=\sum_j|\mu_j|^{1/2}\exp\left(2\pi i f t_{d,j}-i\pi n_j\right)\,, \tag{15}$$

where the magnification of the jth image is $\mu_j=1/\det\left(\partial\boldsymbol{y}/\partial\boldsymbol{x}_j\right)$, $t_{d,j}=t_d(\boldsymbol{x}_j,\,\boldsymbol{y})$, and $n_j=0$, $\frac{1}{2}$, and 1 when $\boldsymbol{x}_j$ is a minimum, saddle, and maximum point, respectively, of $t_d(\boldsymbol{x},\,\boldsymbol{y})$. In the time domain, the wave is expressed as

$$\phi^L(t,\,\boldsymbol{r})=\sum_j|\mu_j|^{1/2}\phi\left(t-t_{d,j},\,\boldsymbol{r}\right)\exp\left(-i\pi n_j\right)\,. \tag{16}$$

This shows that the oscillatory behavior of $F(f)$ at high frequency f is essential to obtain the time delay among the images.

2.1. *Point-Mass Lens*

The surface mass density is expressed as $\Sigma(\boldsymbol{\xi})=M_L\delta^2(\boldsymbol{\xi})$, where M_L is the lens mass. As the normalization constant ξ_0 we adopt the Einstein radius given by $\xi_0=(4M_LD_LD_{LS}/D_S)^{1/2}$, while the nondimensional deflection potential is $\psi(\boldsymbol{x})=\ln x$. In this case equation (11) is analytically integrated as (Peters 1974)

$$F(f)=\exp\left\{\frac{\pi w}{4}+i\frac{w}{2}\left[\ln\left(\frac{w}{2}\right)-2\phi_m(y)\right]\right\}\times\Gamma\left(1-\frac{i}{2}w\right){}_1F_1\left(\frac{i}{2}w,\,1;\,\frac{i}{2}wy^2\right)\,, \tag{17}$$

where $w=8\pi M_{Lz}f$, $\phi_m(y)=(x_m-y)^2/2-\ln x_m$ with $x_m=[y+(y^2+4)^{1/2}]/2$, $M_{Lz}=M_L(1+z_L)$ is the redshifted lens mass, and ${}_1F_1$ is the confluent hypergeometric function. Thus, the amplification factor $F(f)$ includes the two lens parameters: the redshifted lens mass M_{Lz} and the source position y. In the geometrical optics limit ($f\gg M_{Lz}^{-1}$), from equation (15) we have

$$F(f)=|\mu_+|^{1/2}-i|\mu_-|^{1/2}e^{2\pi i f\Delta t_d}\,, \tag{18}$$

where the magnification of each image is $\mu_\pm=1/2\pm(y^2+2)/[2y(y^2+4)^{1/2}]$ and the time delay between double images is $\Delta t_d=4M_{Lz}(y(y^2+4)^{1/2}/2+\ln\{[(y^2+4)^{1/2}+y]/[(y^2+4)^{1/2}-y]\})$. The typical time delay is $\Delta t_d\sim 4M_{Lz}=(2\times10^3\ {\rm s})(M_{Lz}/10^8\ M_\odot)$.

2.2. *Singular Isothermal Sphere*

The surface density of the SIS is characterized by the velocity dispersion v as $\Sigma(\boldsymbol{\xi})=v^2/(2\xi)$. As the normalization constant we adopt the Einstein radius $\xi_0=4\pi v^2D_LD_{LS}/D_S$, and the nondimensional deflection potential is $\psi(\boldsymbol{x})=x$. In this case $F(f)$ in equation (11) is expressed as

$$F(f)=-iwe^{iwy^2/2}\int_0^\infty dx\,xJ_0(wxy)\times\exp\left\{iw\left[\tfrac{1}{2}x^2-x+\phi_m(y)\right]\right\}, \tag{19}$$

where J_0 is the Bessel function of zeroth order; $\phi_m(y)=y+\frac{1}{2}$ and $w=8\pi M_{Lz}f$, where M_{Lz} is defined as the mass inside the Einstein radius given by $M_{Lz}=$

$4\pi^2 v^4(1+z_L)D_L D_{LS}/D_S$. Then, $F(f)$ depends on the two lens parameters M_{Lz} and y. We computed the above integral numerically for various parameters. In the geometrical optics limit ($f \gg M_{Lz}^{-1}$), F is given by

$$F(f) = \begin{cases} |\mu_+|^{1/2} - i|\mu_-|^{1/2} e^{2\pi i f \Delta t_d}\,, & y \le 1\,, \\ |\mu_+|^{1/2}\,, & y \ge 1\,, \end{cases} \qquad (20)$$

where $\mu_\pm = \pm 1 + 1/y$ and $\Delta t_d = 8M_{Lz}y$. If $y \le 1$, double images are formed.

The wave effects in gravitational lensing of gravitational waves have been discussed for a point-mass lens (Nakamura 1998; Ruffa 1999; De Paolis et al. 2002; Zakharov & Baryshev 2002) and a Kerr black hole (Baraldo et al. 1999). However, as far as we know, the wave effects for the SIS model have not been discussed, although the SIS model can be used for more realistic lens objects such as galaxies and star clusters.

2.3. *The Amplification Factor*

In Figure 2 we show the amplification factor $|F(f)|$ as a function of w ($=8\pi M_{Lz} f$) for the fixed source position $y = 0.1$, 0.3, 1, and 3 for the point-mass lens (*left panel*) and the SIS lens (*right panel*). For $w \lesssim 1$, the amplification is very small because of the diffraction effect (e.g., Bontz & Haugan 1981), since in this case the wavelength is so long that the wave does not feel the existence of the lens. For $w \gtrsim 1$, $|F(f)|$ asymptotically converges to the geometrical optics limit (eqs. [18] and [20]),

$$|F(f)|^2 = |\mu_+| + |\mu_-| + 2|\mu_+\mu_-|^{1/2}\sin(2\pi f \Delta t_d)\,, \qquad (21)$$

where $\mu_- = 0$ for $y \ge 1$ in the SIS. The first and second terms in equation (21), $|\mu| = |\mu_+| + |\mu_-|$, represent the total magnification in the geometrical optics. The third term expresses the interference between the double images. The oscillatory behavior (in Fig. 2) is due to this interference. The amplitude and the period of this oscillation are approximately equal to $2|\mu_+\mu_-|^{1/2}$ and $2\pi f \Delta t_d$ in the third term of equation (21), respectively. As the source position y increases, the total magnification $|\mu|$ ($=|\mu_+| + |\mu_-|$) and the amplitude of the oscillation $2|\mu_+\mu_-|^{1/2}$ decrease. This is because each magnification $|\mu_\pm(y)|$ decreases as y increases. We note that even for $y \ge 1$ in the SIS model ($y = 3$ in Fig. 2), the damped oscillatory behavior appears, which looks like a time delay factor of $\sin(2\pi f \Delta t_d)$, although only a single image exists in the geometrical optics limit.

Figure 3 is the same as Figure 2, but we show the phase of the amplification factor $\theta_F(f) = -i\ln[F(f)/|F(f)|]$. The behavior is similar to that of the amplitude (in Fig. 2), and the wave effects appear in the phase θ_F as well as the amplitude $|F|$. For $w \gtrsim 1$, $\theta_F(f)$ asymptotically converges to the geometrical optics limit (eqs. [18] and [20]),

$$\theta_F(f) = \arctan\left[\frac{-|\mu_-|^{1/2}\cos(2\pi f \Delta t_d)}{|\mu_+|^{1/2} + |\mu_-|^{1/2}\sin(2\pi f \Delta t_d)}\right]\,, \qquad (22)$$

where $\mu_- = 0$ for $y \ge 1$ in the SIS. From the above equation (22), the phase θ_F oscillates between $-\arctan(|\mu_-/\mu_+|^{1/2})$ and $\arctan(|\mu_-/\mu_+|^{1/2})$ with a period of $2\pi f \Delta t_d$. As the source position y increases, the magnification ratio $|\mu_-/\mu_+|$ and the amplitude of the oscillation $\arctan(|\mu_-/\mu_+|^{1/2})$ decrease.

3. GRAVITATIONALLY LENSED WAVEFORM AND PARAMETER ESTIMATION

3.1. *Gravitational-Wave Measurement with LISA*

We briefly discuss gravitational-wave measurement with *LISA* (see Cutler 1998; Bender et al. 2000). *LISA* consists of three spacecrafts forming an equilateral triangle and orbits around the Sun, trailing 20° behind the Earth. The sides of the triangle are $L = 5 \times 10^6$ km in length, and the plane of

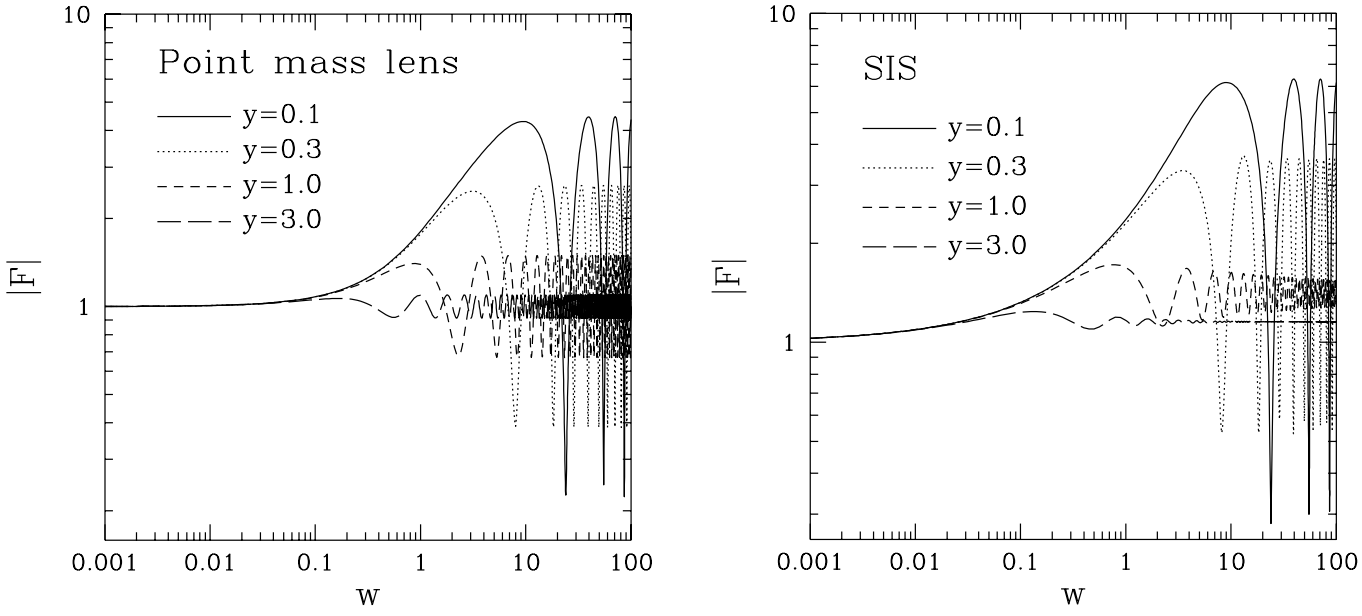

FIG. 2.—Amplification factor $|F(f)|$ as a function of w ($=8\pi M_{Lz} f$) with the fixed source position $y = 0.1$, 0.3, 1, and 3 for a point-mass lens (*left*) and an SIS (*right*). For $w \lesssim 1$, the amplification is very small because of the diffraction effect. For $w \gtrsim 1$, the oscillatory behavior appears because of the interference between the double images. We note for the SIS that even if $y \ge 1$ (a single image is formed in the geometrical optics limit), the damped oscillatory behavior appears.

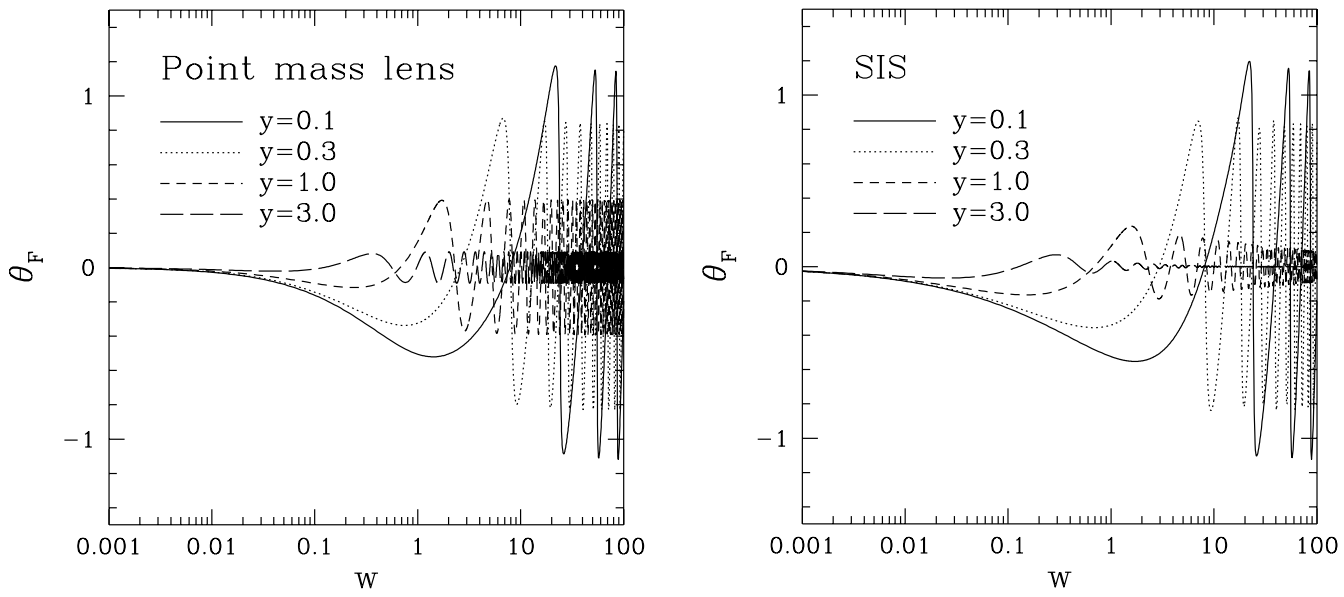

FIG. 3.—Same as Fig. 2, but for the phase of the amplification factor $\theta_F(f) = -i \ln[F(f)/|F(f)|]$ as a function of $w\,(=8\pi M_{Lz} f)$

the triangle is inclined at 60° with respect to the ecliptic. The triangle rotates annually. The gravitational-wave signal is reconstructed from three data streams that effectively correspond to three time-varying arm lengths. Any two of the three data streams are linearly independent of each other. The data contain both gravitational-wave signals to be fitted by matched filtering and noise signals that are assumed to be stationary, Gaussian, and uncorrelated with each other (Cutler 1998). The gravitational-wave signals $h_{\rm I,II}(t)$ from a binary are written as

$$h_{\rm I,II}(t) = \frac{\sqrt{3}}{2}\left[F^{+}_{\rm I,II}(t)h_{+}(t) + F^{\times}_{\rm I,II}(t)h_{\times}(t)\right] , \qquad (23)$$

where $F^{+,\times}_{\rm I,II}(t)$ are pattern functions that depend on the angular position of the binary, its orientation, and the detector's configuration. The quantities $h_{+,\times}(t)$ are the two polarization modes of gravitational radiation from the binary. The direction and the orientation of the binary and the direction of the lens are assumed to be constant during the observation in the fixed barycenter frame of the solar system. Further discussion and details about the pattern functions are given in Cutler (1998).

3.2. *Gravitationally Lensed Signal Measured by LISA*

We consider the SMBH binaries at redshift z_S as the sources. We use a restricted post-Newtonian approximation as the in-spiral waveform (Cutler & Flanagan 1994). The coalescing time for a circular orbit is typically $t_c = (0.1\ {\rm yr})(\mathscr{M}_z/10^6\ M_\odot)^{-5/3}(f/10^{-4}\ {\rm Hz})^{-8/3}$, where $\mathscr{M}_z = (M_1 M_2)^{3/5}(M_1 + M_2)^{-1/5}(1 + z_S)$ is the redshifted chirp mass. At the solar system barycenter, the unlensed waveforms $\tilde{h}_{+,\times}(f)$ in the frequency domain are given by

$$\tilde{h}_{+}(f) = A\left[1 + (\boldsymbol{L}\cdot\boldsymbol{n})^2\right] f^{-7/6} e^{i\Psi(f)} ,$$
$$\tilde{h}_{\times}(f) = -2iA(\boldsymbol{L}\cdot\boldsymbol{n}) f^{-7/6} e^{i\Psi(f)} , \qquad (24)$$

where $\boldsymbol{L}$ (given by $\bar{\theta}_L$, $\bar{\phi}_L$) is the unit vector in the direction of the binary's orbital angular momentum and $\boldsymbol{n}$ (given by $\bar{\theta}_S$, $\bar{\phi}_S$) is the unit vector toward the binary. These vectors are defined in the fixed barycenter frame of the solar system. The amplitude A and the phase $\Psi(f)$ depend on six parameters: the redshifted chirp mass $\mathscr{M}_z$, the reduced mass $\mu_z = M_1 M_2(1 + z_S)/(M_1 + M_2)$, the spin-orbit coupling constant β, the coalescence time t_c, the phase ϕ_c, and the angular diameter distance to the source D_S. The amplitude is

$$A = \sqrt{\frac{5}{96}}\frac{\pi^{-2/3}\mathscr{M}_z^{5/6}}{D_S(1 + z_S)^2} , \qquad (25)$$

where $D_S(1 + z_S)^2$ is the luminosity distance to the source and $\Psi(f)$ is a rather complicated function of $\mathscr{M}_z$, μ_z, β, ϕ_c, and t_c (see Cutler & Flanagan 1994, eq. [3.24]).

The gravitationally lensed waveforms $\tilde{h}^L_{+,\times}(f)$ in the frequency domain are given by the product of the amplification factor $F(f)$ and the unlensed waveforms $\tilde{h}_{+,\times}(f)$ (see § 2):

$$\tilde{h}^L_{+,\times}(f) = F(f)\tilde{h}_{+,\times}(f) , \qquad (26)$$

where the function $F(f)$ is given in equation (11). Using equations (23), (24), and (26), the observed lensed signals $\tilde{h}^L_\alpha(f)$ ($\alpha = {\rm I, II}$) with *LISA* are given in the stationary phase approximation as

$$\tilde{h}^L_\alpha(f) = \frac{\sqrt{3}}{2}\frac{D_S\xi_0^2(1 + z_L)}{D_L D_{LS}}\frac{f}{i}\int d^2\boldsymbol{x}\,\Lambda_\alpha(t + t_d(\boldsymbol{x},\ \boldsymbol{y}))$$
$$\times e^{2\pi i f t_d(\boldsymbol{x},\boldsymbol{y})} e^{-i\left(\phi_{\rm D} + \phi_{p,\alpha}\right)[t + t_d(\boldsymbol{x},\boldsymbol{y})]} A f^{-7/6} e^{i\Psi(f)} , \qquad (27)$$

where

$$\phi_{p,\alpha}(t) = \tan^{-1}\left\{\frac{2(\boldsymbol{L}\cdot\boldsymbol{n})F^{\times}_\alpha(t)}{[1 + (\boldsymbol{L}\cdot\boldsymbol{n})^2]F^{+}_\alpha(t)}\right\}$$

$$\Lambda_\alpha(t) = \left\{(2\boldsymbol{L}\cdot\boldsymbol{n})^2 F^{\times 2}_\alpha(t) + \left[1 + (\boldsymbol{L}\cdot\boldsymbol{n})^2\right]^2 F^{+2}_\alpha(t)\right\}^{1/2} .$$

The Doppler phase is

$$\phi_{\rm D}(t) = 2\pi f(t) R \sin\bar{\theta}_S \cos\left(\bar{\phi}(t) - \bar{\phi}_S\right) ,$$

$R = 1$ AU, and $\bar{\phi}(t) = 2\pi t/T$ ($T = 1$ yr), where $t = t(f)$ is given in equation (3.10) of Cutler & Flanagan (1994). In the no-lens limit of $\psi(\boldsymbol{x}) = 0$, the lensed signals $\tilde{h}^L_\alpha(f)$ in equation (27) agree with the unlensed ones $\tilde{h}_\alpha(f)$ in Cutler (1998). We assume the source position $\boldsymbol{y}$ is constant during the observation, since the characteristic scale of the interference pattern, $\sim(10^7\ \mathrm{AU})(M_{Lz}/10^8\ M_\odot)^{-1/2}(f/\mathrm{mHz})^{-1} \times [(D_S D_L/D_{LS})/\mathrm{Gpc}]^{1/2}$, is extremely larger than *LISA*'s orbital radius (1 AU).

Since the lensed signals $\tilde{h}^L_\alpha(f)$ in equation (27) are given by a double integral, we approximate $\tilde{h}^L_\alpha(f)$ in two limiting cases: (1) the geometrical optics limit ($f \gg t_d^{-1}$) and (2) the time delay being much smaller than *LISA*'s orbital period ($t_d \ll 1$ yr). In the geometrical optics limit, from equation (15) we obtain

$$\tilde{h}^L_\alpha(f) = \frac{\sqrt{3}}{2}\sum_j |\mu_j|^{1/2}\Lambda_\alpha(t + t_{d,j})e^{2\pi i f t_{d,j} - i\pi n_j} \times e^{-i(\phi_D + \phi_{p,\alpha})(t+t_{d,j})} A f^{-7/6} e^{i\Psi(f)} . \quad (28)$$

If the time delay is much smaller than *LISA*'s orbital period ($t_d \ll 1$ yr), we expand Λ_α, ϕ_D, and $\phi_{p,\alpha}$ around $t_d = 0$ to get

$$\tilde{h}^L_\alpha(f) = \frac{\sqrt{3}}{2}\Lambda_\alpha(t)e^{-i(\phi_D+\phi_{p,\alpha})(t)} A f^{-7/6} e^{i\Psi(f)} \times \left\{ F(f) + \frac{d}{dt}\left[\ln\Lambda_\alpha - i(\phi_D + \phi_{p,\alpha})\right]\frac{f}{2\pi i}\frac{d}{df} \times \left[\frac{F(f)}{f}\right] + O\left[\left(\frac{t_d}{1\ \mathrm{yr}}\right)^2\right]\right\} . \quad (29)$$

Since we consider a lens mass $M_{Lz} = 10^6$–$10^9\ M_\odot$, the time delay is much smaller than 1 yr. Thus, we use the above equation (29) as the lensed waveforms for the following calculations.

In Figure 4 the lensed signals $|\tilde{h}^L_\alpha(f)|$ ($\alpha = \mathrm{I}, \mathrm{II}$) and the unlensed ones $|\tilde{h}_\alpha(f)|$ are shown. We show the results from 1 yr before the final merging to the innermost stable circular orbit [the binary separation is $r = 6(M_1 + M_2)$]. We set typical parameters of the SMBH binary masses $M_{1,2z} = 10^6\ M_\odot$, the lens mass $M_{Lz} = 10^8\ M_\odot$, and the source position $y = 1$ for the point-mass lens. The angular parameters are $\cos\bar{\theta}_S = 0.3$, $\bar{\phi}_S = 5.0$, $\cos\bar{\theta}_L = 0.8$, and $\bar{\phi}_L = 2.0$, and the source redshift is $z_S = 1$ (the angular diameter distance is $H_0 D_S = 0.386$). Therefore, the frequency range is from 5×10^{-5} to 2×10^{-3} Hz, and the time delay is 4×10^3 s. The strange behavior in the lower frequency $f \lesssim 10^{-4}$ Hz is due to *LISA*'s orbital motion. In this frequency region, however, the difference between the lensed signal and the unlensed one is small because of diffraction (see Fig. 2). On the other hand, the oscillatory behavior appears in the higher frequency region $f \gtrsim 10^{-4}$ Hz. This critical frequency is determined by the inverse of the lens mass $8\pi M_{Lz}$ (see Fig. 2). The oscillatory amplitude and the period are determined by the product of the magnifications $2|\mu_+\mu_-|^{1/2} = 2/[y(y^2+4)^{1/2}]$ and the inverse of the time delay, $1/\Delta t_d$ (see the third term of eq. [21]).

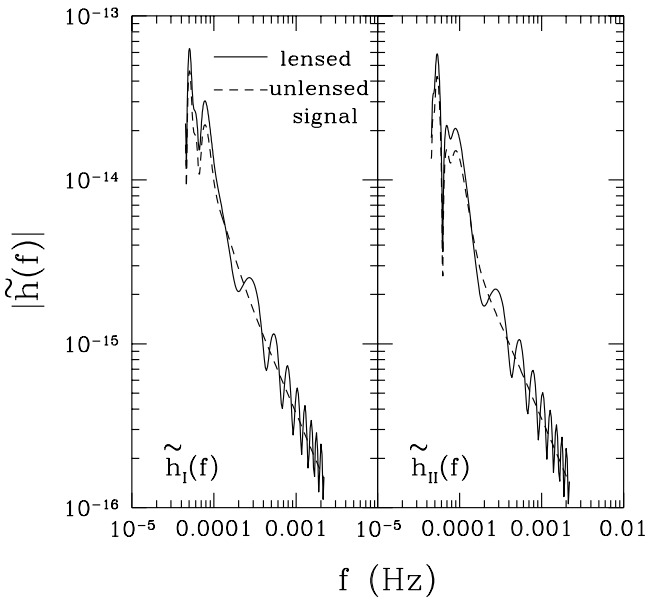

FIG. 4.—Lensed signals $|\tilde{h}^L_\alpha(f)|$ ($\alpha = \mathrm{I}, \mathrm{II}$) (*solid line*) and unlensed ones $|\tilde{h}_\alpha(f)|$ (*dashed line*) measured by *LISA*. The signals are shown from 1 yr before coalescence to the innermost stable circular orbit of $r = 6(M_1 + M_2)$. The redshifted masses of the SMBH binary $M_{1,2z} = 10^6\ M_\odot$, the redshifted lens mass $M_{Lz} = 10^8\ M_\odot$, and the source position $y = 1$. The angular parameters are $\cos\bar{\theta}_S = 0.3$, $\bar{\phi}_S = 5.0$, $\cos\bar{\theta}_L = 0.8$, $\bar{\phi}_L = 2.0$, and the source redshift is $z_S = 1$ (the distance is $H_0 D_S = 0.386$). The strange behavior for $f \lesssim 10^{-4}$ Hz is due to the *LISA* orbital motion, and the difference between the two signals is small because of diffraction. On the other hand, the oscillatory behavior appears for $f \gtrsim 10^{-4}$ Hz, which is determined by the inverse of the lens mass $8\pi M_{Lz}$ (see Fig. 2). This oscillation is due to the interference between the double images.

3.3. *Parameter Extraction*

We briefly mention the matched filtering analysis and the parameter estimation errors (Finn 1992; Cutler & Flanagan 1994). We assume that the signal $\tilde{h}^L_\alpha(f)$ is characterized by some unknown parameters γ_i. In the present case, there are 10 source parameters ($\mathcal{M}_z$, μ_z, β, ϕ_c, t_c, D_S, $\bar{\theta}_S$, $\bar{\phi}_S$, $\bar{\theta}_L$, $\bar{\phi}_L$) and two lens parameters (M_{Lz}, y). In the matched filtering analysis the variance-covariance matrix of the parameter estimation error $\Delta\gamma_i$ is given by inverse of the Fisher information matrix Γ_{ij} as $\langle\Delta\gamma_i\Delta\gamma_j\rangle = (\Gamma^{-1})_{ij}$. The Fisher matrix becomes

$$\Gamma_{ij} = 4\sum_{\alpha=\mathrm{I,II}} \mathrm{Re}\int \frac{df}{Sn(f)}\frac{\partial\tilde{h}^{L*}_\alpha(f)}{\partial\gamma_i}\frac{\partial\tilde{h}^L_\alpha(f)}{\partial\gamma_j} , \quad (30)$$

where $Sn(f)$ is the noise spectrum. The noise spectrum $Sn(f)$ is the sum of the instrumental and the confusion noise, and we adopt the same noise spectrum as in Cutler (1998). The S/N is given by

$$(\mathrm{S/N})^2 = 4\sum_{\alpha=\mathrm{I,II}}\int\frac{df}{Sn(f)}|\tilde{h}^L_\alpha(f)|^2 . \quad (31)$$

We computed the variance-covariance matrix Γ_{ij} for a wide range of the lens parameters (M_{Lz}, y), using the lensed waveform in equation (29). Since the S/N is very high for the SMBH merger, the Fisher matrix approach to calculating the estimation errors is valid (Cutler 1998). We integrate the gravitationally lensed waveform (in eqs. [30] and [31]) from 1 yr before the final merging to the cutoff frequency f_{cut} when the binary separation becomes $r = 6(M_1 + M_2)$. We do not consider the low-frequency cutoff of *LISA*, which is the low-frequency noise wall of space-based instruments and is around 10^{-5} to 10^{-4} Hz (Vecchio 2003). This

assumption is to underestimate the errors in the estimation parameters.

4. RESULTS

In this section we present numerical results to compute the S/N and the errors in estimation parameters. We randomly distribute 100 binaries over various directions and orientations on celestial spheres at $z_S = 1$ (the distance is $H_0 D_S = 0.386$). We present the mean value averaged for 100 binaries.

4.1. *Lensing Effects on the Signal-to-Noise Ratio*

We demonstrate the gravitational lensing effect on the S/N. In Figure 5 the increasing factor of S/N by gravitational lensing for the point-mass lens is shown for the fixed source positions $y = 0.1$, 0.3, 1, and 3 as a function of the lens mass M_{Lz}. The vertical axis is the S/N with the gravitational lensing divided by the unlensed S/N. Four panels are shown for the various SMBH binary masses: $M_{1,2z} = 10^4$, 10^5, 10^6, and 10^7 $M_\odot$. We show the mean value averaged for 100 binaries, but the dispersion is negligibly small (<5%). For a lens mass smaller than 10^6 $M_\odot$, the magnification is

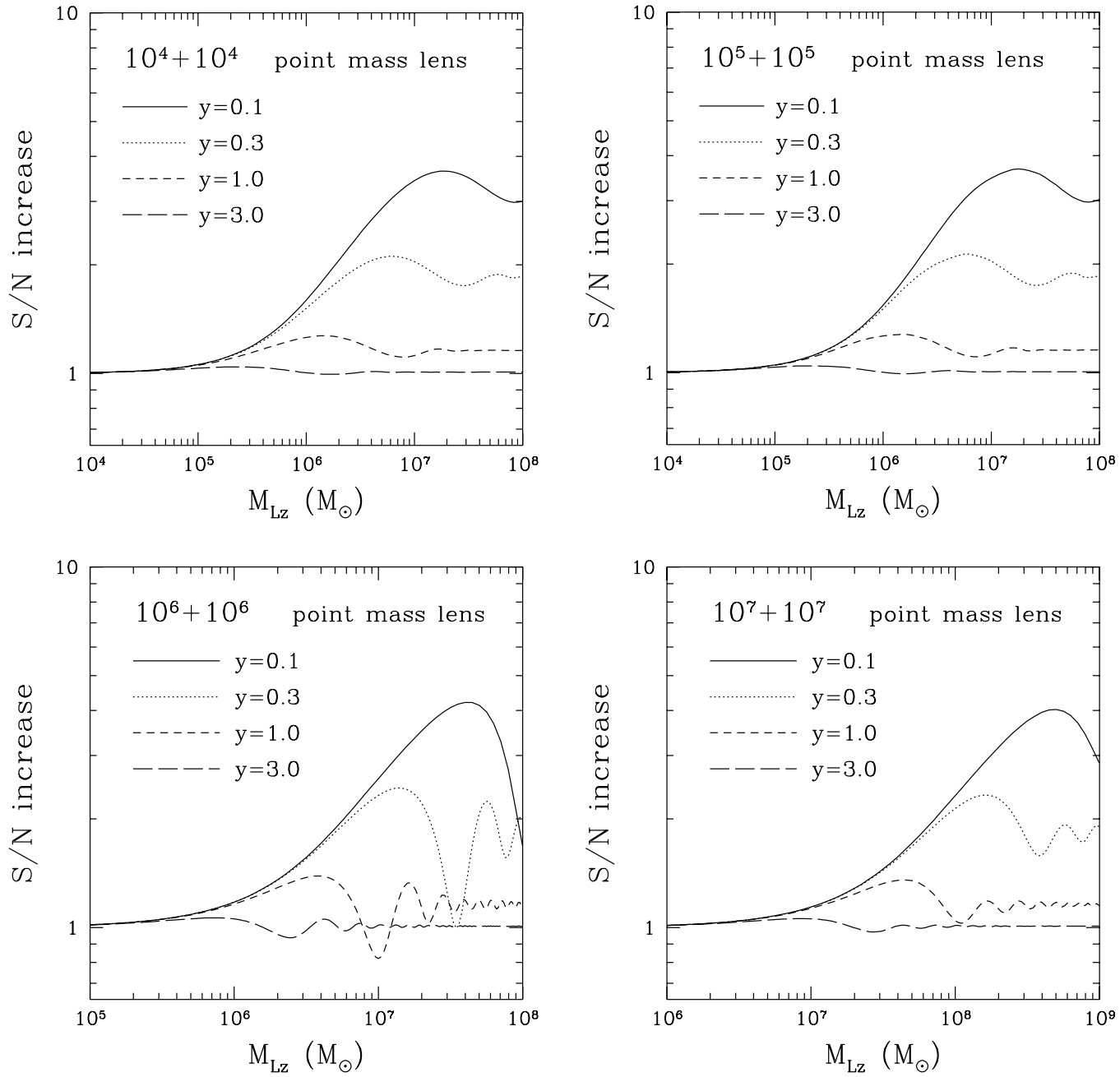

FIG. 5.—Increasing factor in S/N due to the gravitational lensing by the point-mass lens for various SMBH binary masses: $M_{1,2z} = 10^4$, 10^5, 10^6, and 10^7 $M_\odot$. The horizontal axis is the redshifted lens mass; the vertical axis is the lensed S/N divided by the unlensed S/N. The source position is fixed at $y = 0.1$, 0.3, 1, and 3. For $M_{Lz} \lesssim 10^6$ $M_\odot$, the magnification is very small because of the diffraction effect irrespective of the SMBH binary masses. For $M_{Lz} \gtrsim 10^7$ $M_\odot$, the damped oscillatory patterns appear because of the interference between the two images, and this behavior converges in the geometrical optics limit, $|\mu|^{1/2} = (y^2+2)^{1/2}/[y^{1/2}(y^2+4)^{1/4}]$.

very small irrespective of the SMBH binary masses because of diffraction effects. In this case the Schwarzschild radius of the lens mass M_{Lz} is smaller than the wavelength of the gravitational waves $\lambda \sim 1$ AU, and the waves are not magnified by lensing. This critical lens mass ($10^6\ M_\odot$) is mainly determined by the inverse of the knee frequency of *LISA*'s noise spectrum, $1/(8\pi f) \sim (8 \times 10^6\ M_\odot)(f/\mathrm{mHz})^{-1}$ (see Fig. 2), but for $10^7 + 10^7\ M_\odot$, the SMBH binary coalesces at a lower frequency ($f \sim 10^{-4}$ Hz); thus, the critical lens mass is shifted for a larger mass ($10^7\ M_\odot$), as shown in the bottom right panel of Figure 5. This tells us that if the lens mass is smaller than $10^6\ M_\odot$, the effect of the lens is very small. If the lens mass is larger than $10^7\ M_\odot$, the damped oscillatory behavior appears because of the interference between the two images, and the S/N converges to the geometrical optics limit, $|\mu|^{1/2} = (y^2+2)^{1/2}/[y^{1/2}(y^2+4)^{1/4}]$, which is independent of the lens mass. As y increases from 0.1 (*solid line*) to 3 (*dashed line*), the amplification decreases, since the magnifications of the two images [$|\mu_\pm(y)|$] decrease as y increases (see also Fig. 2).

Figure 6 is the same as Figure 5, but for the SIS lens model. The behavior is very similar to that in the point-mass lens. For a lens mass larger than $10^7\ M_\odot$, the S/N converges to the geometrical optics limit, $|\mu|^{1/2} = (2/y)^{1/2}$ for $y \leq 1$

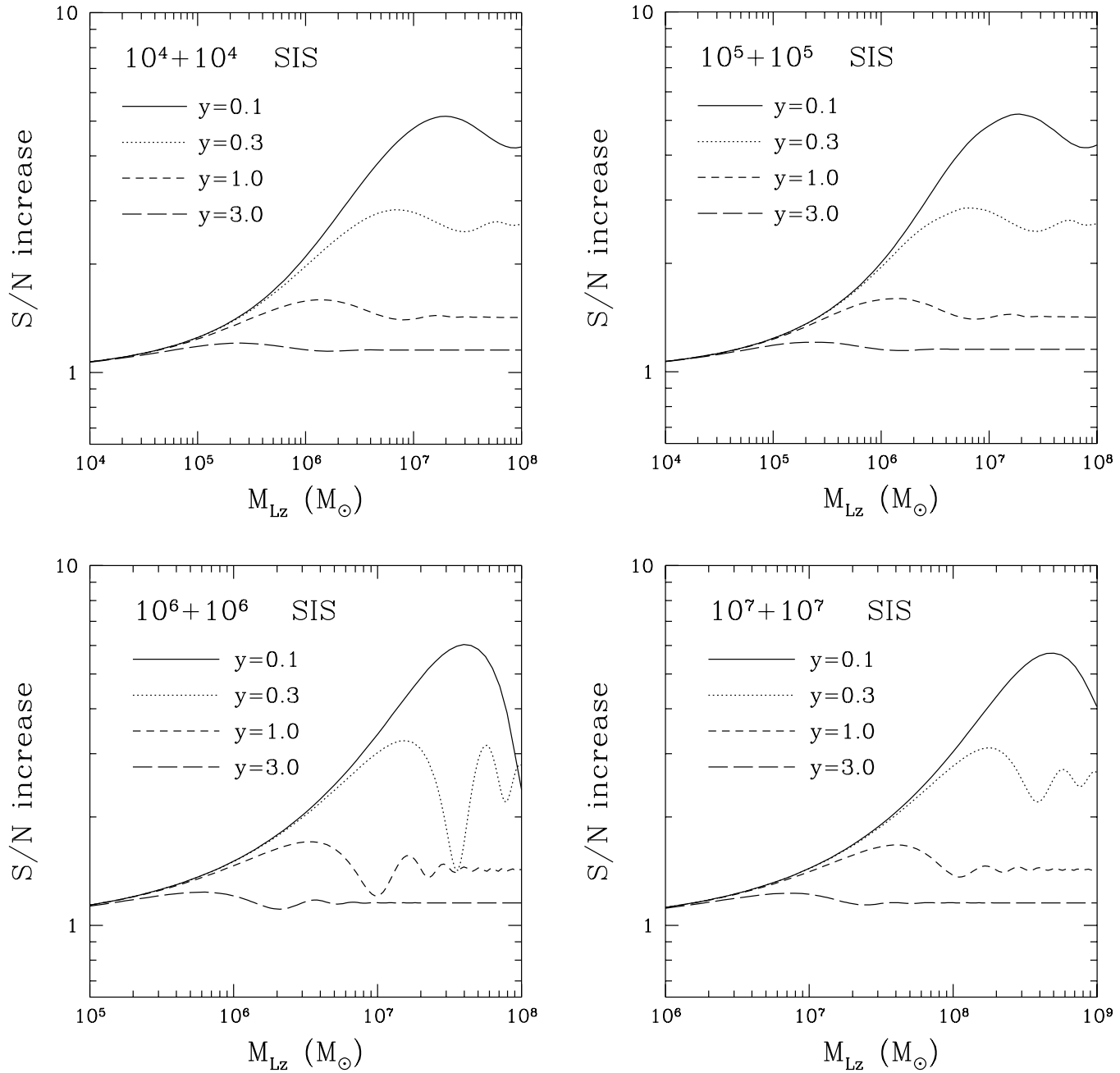

FIG. 6.—Same as Fig. 5, but for the SIS lens model. For $M_{Lz} \gtrsim 10^7\ M_\odot$, the results converge in the geometrical optics limit: $|\mu|^{1/2} = (2/y)^{1/2}$ for $y \leq 1$ and $|\mu|^{1/2} = (1+1/y)^{1/2}$ for $y \geq 1$.

and $|\mu|^{1/2} = (1 + 1/y)^{1/2}$ for $y \geq 1$. As y increases from 0.1 (*solid line*) to 3 (*dashed line*), the amplification decreases (see also the right panel of Fig. 2).

4.2. *Parameter Estimation for the Lens Objects*

In this section we show the parameter estimation for the lens objects. We show the results for an SMBH binary with masses $10^6 + 10^6\ M_\odot$, because we found the S/N to be higher than with other binary masses ($M_{1,2z} = 10^4$, 10^5, and $10^7\ M_\odot$). We distribute 100 binaries over various directions and orientations at $z_S = 1$, and the mean value of the S/N without lensing is 2600 in these 100 binaries. We show the mean value of errors averaged for the 100 binaries; for $M_{Lz} \lesssim 10^7\ M_\odot$ the dispersion is relatively large ($\lesssim 40\%$), but for $M_{Lz} \gtrsim 10^7\ M_\odot$ the results converge to that in the geometrical optics limit, and the dispersion is negligibly small.

In Figure 7 the estimation errors for the redshifted lens mass ΔM_{Lz} (*left panel*) and the source position Δy (*right panel*) are shown as a function of M_{Lz} with $y = 0.1$, 0.3, 1, and 3 for the point-mass lens. We use units of $\mathrm{S/N} = 10^3$, and the results (ΔM_{Lz}, Δy) scale as $(\mathrm{S/N})^{-1}$. For $M_{Lz} \lesssim 10^7\ M_\odot$, the estimation errors are relatively large ($\gtrsim 10\%$), since the effect of lensing on the signals is very small because of diffraction. For $M_{Lz} \gtrsim 10^8\ M_\odot$, the geometrical optics approximation is valid, and the errors converge to a constant in Figure 7. The redshifted lens mass and the source position can be determined up to an accuracy of $\sim 0.1\%$, as shown in Figure 7. The errors in the geometrical optics limit are well fitted by (see the Appendix)

$$\frac{\Delta M_{Lz}}{M_{Lz}} = \frac{1}{\mathrm{S/N}} \frac{\sqrt{y(y^2+2)}(y^2+4)^{5/4}}{2\tau}\ ,$$
$$\frac{\Delta y}{y} = \frac{1}{\mathrm{S/N}} \frac{\sqrt{y^2+2}(y^2+4)^{3/4}}{2\sqrt{y}}\ , \qquad (32)$$

where S/N is in the unlensed case, and

$$\tau = \Delta t_d / 4M_{Lz} = y(y^2+4)^{1/2}/2 + \ln\{[(y^2+4)^{1/2} + y]/[(y^2+4)^{1/2} - y]\}\ .$$

Thus, one could determine the lens parameters, the redshifted lens mass and the source position, up to an accuracy of $\sim(\mathrm{S/N})^{-1}$. The above equations (32) are valid if the time delay Δt_d is much smaller than *LISA*'s orbital period of 1 yr. If the time delay Δt_d becomes comparable to 1 yr, *LISA*'s orbital motion affects the results.

Figure 8 is the same as Figure 7, but as a function of y. For $y \gtrsim 1$, the errors are convergent to the geometrical optics limit of equations (32) irrespective of the lens mass. As y increases, the time delay t_d increases, and the geometrical optics limit ($f t_d \gg 1$) is valid. We note that even for $y \gtrsim 10$, one can extract the lens information. In the case of light the observable is the lensed flux, which is proportional to the magnifications, $\propto |\mu_\pm|$, but for gravitational waves the observable is the lensed amplitude, which is proportional to the square root of the magnifications, $\propto |\mu_\pm|^{1/2}$. For example, let us consider the case in which the flux ratio of a brighter image to a fainter one is 100 : 1. Then, the amplitude ratio is 10 : 1, so that the fainter image can be observed even if the source position is far from the Einstein radius in the case of gravitational waves. Denoting the largest source position for which one can extract the lens parameters as y_{cr}, we approximate the errors in equations (32) for the large-y limit: $\Delta\gamma/\gamma \simeq (\mathrm{S/N})^{-1} y^2$, where $\gamma = M_{Lz}, y$. Then, we obtain

$$y_{\mathrm{cr}} \simeq 10 \left(\frac{\Delta\gamma/\gamma}{0.1}\right)^{1/2} \left(\frac{\mathrm{S/N}}{10^3}\right)^{1/2}\ . \qquad (33)$$

Thus, the lensing cross section ($\propto y_{\mathrm{cr}}^2$) increases by an order of magnitude more than that for the usual strong lensing of light ($y_{\mathrm{cr}} = 1$; e.g., Turner, Ostriker & Gott 1984).

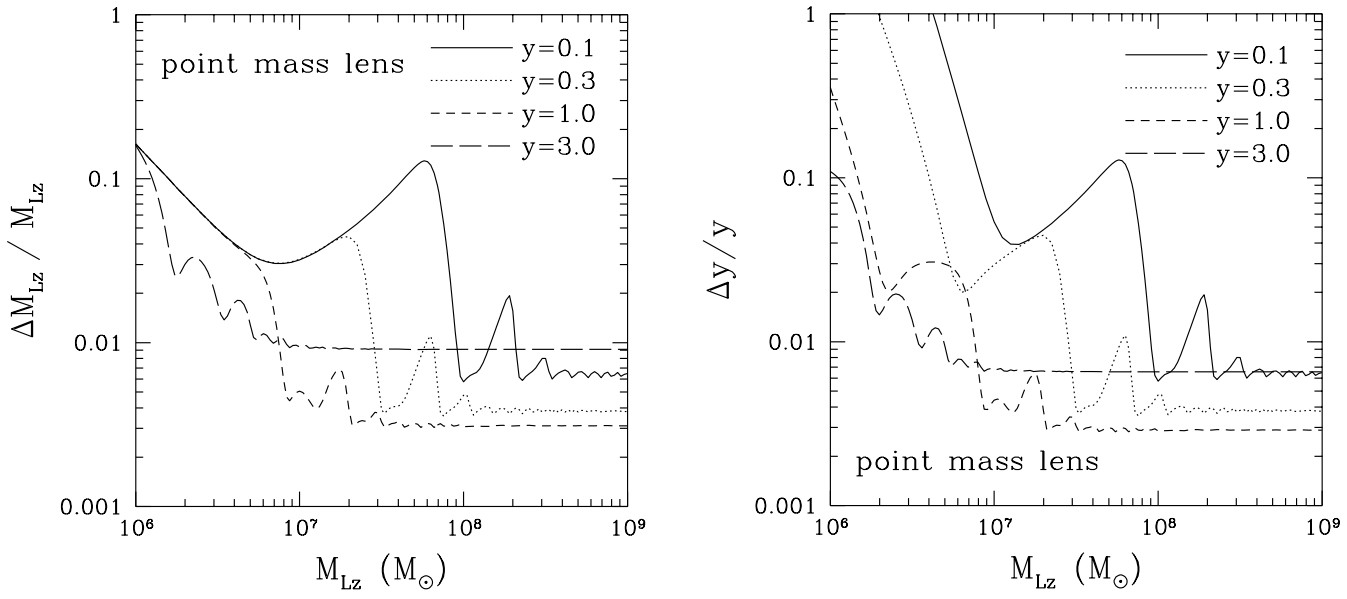

FIG. 7.—Estimation errors for the redshifted lens mass ΔM_{Lz} (*left*) and the source position Δy (*right*) for the point-mass lens. The results are presented for an SMBH binary of masses $10^6 + 10^6\ M_\odot$ at $z_S = 1$. The errors are normalized by $\mathrm{S/N} = 10^3$ and simply scale as $(\mathrm{S/N})^{-1}$. For $M_{Lz} \lesssim 10^7\ M_\odot$, the errors are relatively large, since the effect of lensing is very small because of diffraction. For $M_{Lz} \gtrsim 10^8\ M_\odot$, the geometrical optics approximation is valid, and errors converge to constants.

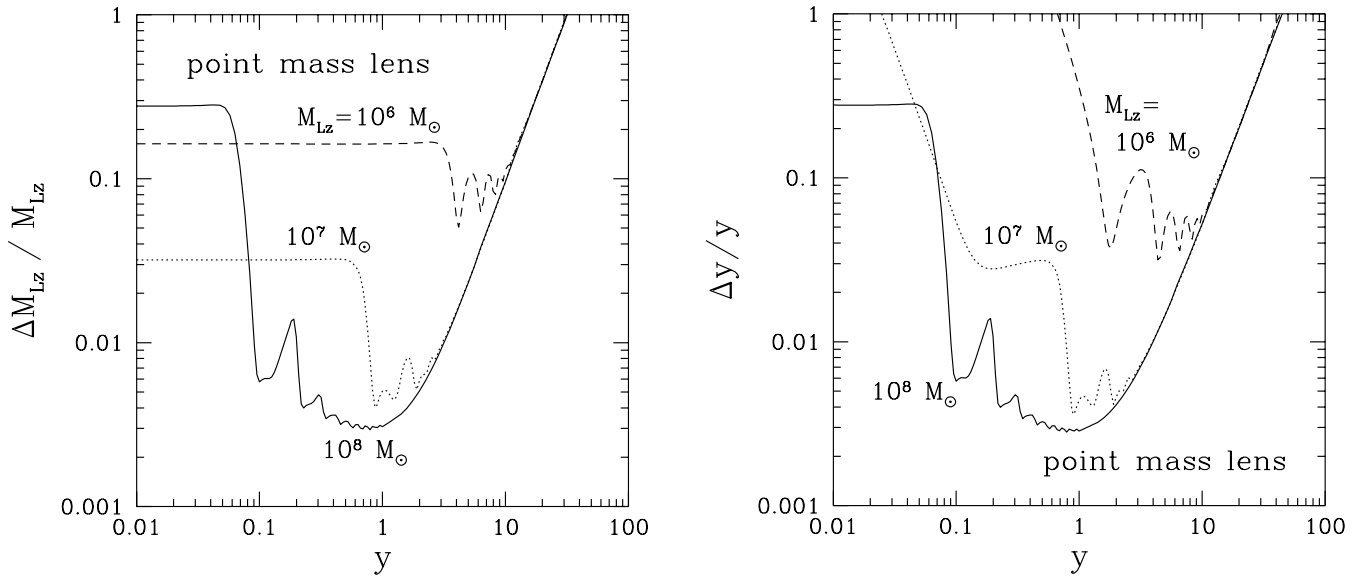

FIG. 8.—Same as Fig. 7, but as a function of y. We note that even for $y \gtrsim 10$, we can extract the lens information. Then, the lensing cross section ($\propto y^2$) increases by an order of magnitude more than for the usual strong lensing of light ($y = 1$).

In Figure 9 the estimation errors for the SIS model are shown. For $M_{Lz} \lesssim 10^7\ M_\odot$, the behavior is similar to the point-mass lens, but for $M_{Lz} \gtrsim 10^8\ M_\odot$, the behavior strongly depends on y. In the geometrical optics approximation, the errors are given by (see the Appendix)

$$\frac{\Delta M_{Lz}}{M_{Lz}} = \frac{\Delta y}{y} = \frac{1}{\mathrm{S/N}} \sqrt{\frac{2(1-y^2)}{y}} \quad \text{for } y \le 1\ , \qquad (34)$$

and the lens parameters are not determined for $y \ge 1$. We note that even for $y = 3$, the lens parameters can be extracted for $M_{Lz} \sim 10^6$–$10^8\ M_\odot$ because of the wave effects. For $y = 0.1$ and 0.3, the asymptotic behavior of the errors is somewhat smaller than the results in equation (34), because the order of $1/f$ term in $F(f)$ (which is neglected in the geometrical optics approximation $f \to \infty$) affects the results. For $y = 1$, the errors decrease as lens mass increases, as shown in Figure 9, because the errors converge to the results in the geometrical optics limit of equation (34), which vanish at $y = 1$. As a result, if $y > 1$, the errors asymptotically increase with the increase of the lens mass, but if $y < 1$, they asymptotically converge to constants.

Figure 10 is the same as Figure 9, but as a function of y. We note that even for larger $y \gtrsim 1$, we can extract the lens information. Thus, the lensing probability ($\propto y^2$) to determine the lens parameters increases as compared to the results in the geometrical optics limit for lens objects in the mass range 10^6–$10^8\ M_\odot$.

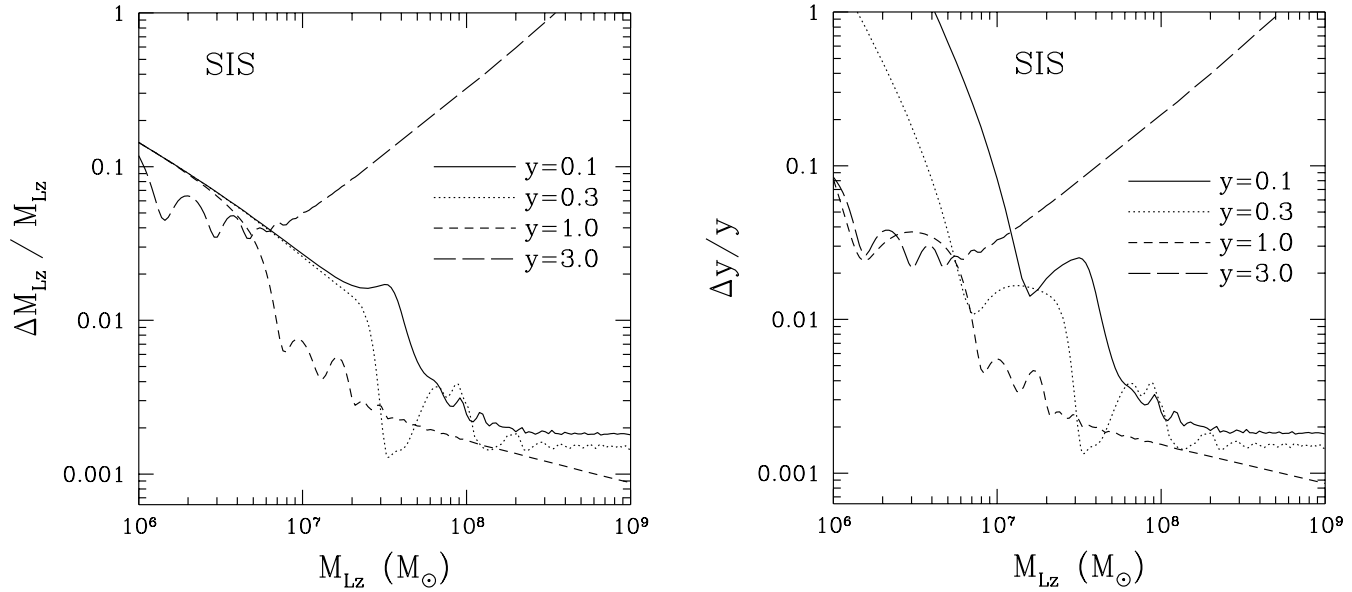

FIG. 9.—Estimation errors for the redshifted lens mass ΔM_{Lz} (*left*) and the source position Δy (*right*) for the SIS model. The results are presented for an SMBH binary of masses $10^6 + 10^6\ M_\odot$ at $z_S = 1$. The errors are normalized by $\mathrm{S/N} = 10^3$ and simply scale as $(\mathrm{S/N})^{-1}$. Even for $y = 3$ (a single image is formed in the geometrical optics limit), the lens parameters can be extracted at $M_{Lz} \sim 10^6$–$10^8\ M_\odot$ because of wave effects.

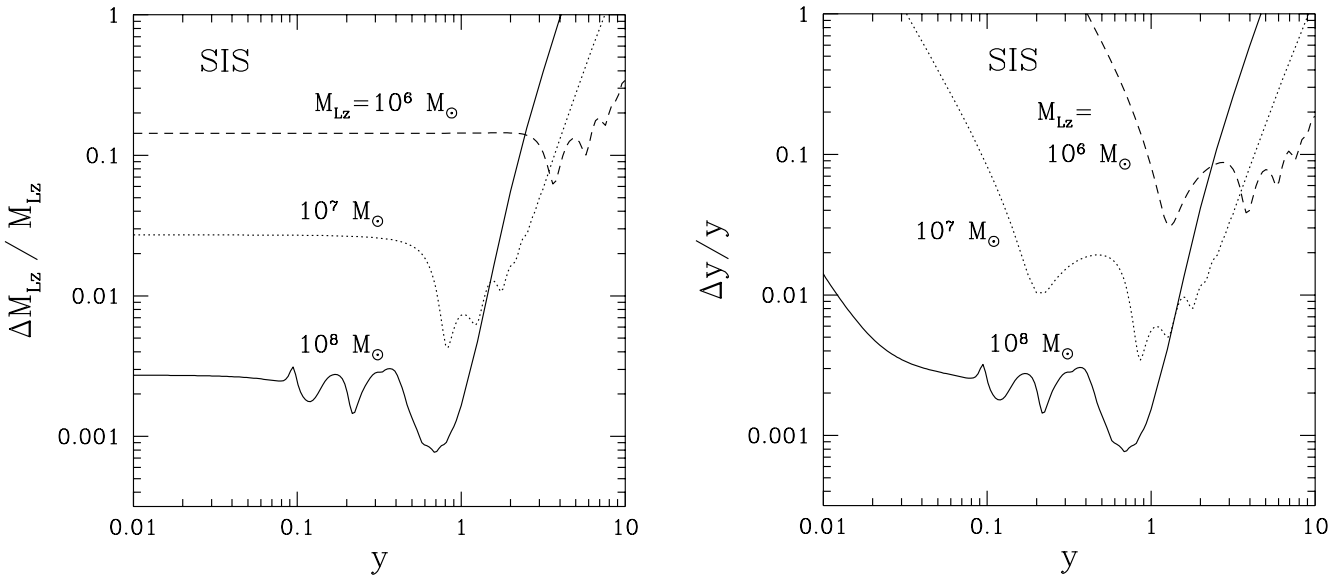

FIG. 10.—Same as Fig. 9, but as a function of y. We note that even for $y > 1$, we can determine the lens parameters. Then, the lensing cross section ($\propto y^2$) becomes larger than that in the geometrical optics approximation ($y = 1$).

4.3. *Lensing Effects on the Estimation Errors of the Binary Parameters*

We discuss the gravitational lensing effects on the estimation errors of the SMBH binary parameters. We study five binary parameters: the redshifted chirp mass $\mathcal{M}_{cz}$, the reduced mass μ_z, the distance to the source D_S, and the angular resolution ($\bar{\theta}_S$, $\bar{\phi}_S$). We find that the estimation errors of these parameters decrease because S/N increases by lensing (see Figs. 5 and 6). The error $\Delta\gamma$ is roughly proportional to the inverse of the S/N as $\Delta\gamma \propto (\mathrm{S/N})^{-1}$ (see eqs. [30] and [31]).

4.4. *Results for Various SMBH Masses and Redshifts*

So far we have presented the results for equal-mass SMBH binaries with redshift $z_S = 1$. In this section we comment on the results for the case of various (unequal) SMBH masses of 10^4–$10^7\ M_\odot$ and redshifts $z_S = 1$–10.

The critical lens mass at which the wave effects become important (10^6–$10^8\ M_\odot$) is mainly determined by the inverse of the knee frequency of *LISA*'s noise spectrum, $\sim(8 \times 10^6\ M_\odot)(f/\mathrm{mHz})^{-1}$, independent of the binary mass (see § 4.1). However, for a massive binary of total mass $(M_{1z} + M_{2z}) \gtrsim 10^7\ M_\odot$, the binary coalesces at a lower frequency ($\sim 10^{-4}$ Hz); thus, the critical lens mass is shifted for a larger mass (10^7–$10^9\ M_\odot$). For a larger lens mass $M_{Lz} \gtrsim 10^8\ M_\odot$, the results (the S/N increase and the estimation errors) converge to that in the geometrical optics limit irrespective of the binary mass. The estimation errors in Figures 7–10 are for the case of a $10^6 + 10^6\ M_\odot$ binary at redshift $z_S = 1$ and are normalized to $\mathrm{S/N} = 10^3$ and simply scale as $(\mathrm{S/N})^{-1}$. In order to translate the results in the various unequal SMBH binaries, we present the S/N for binary masses $M_{1,2z} = 10^4$–$10^7\ M_\odot$ with redshifts $z_S = 1$, 3, 5, and 10 in Table 1. We assume a 1 yr observation of in-spiral phase before final merging. The results are the mean value of 100 binaries that are randomly distributed at each redshift, and the dispersion is relatively large ($\sim$50%). From Table 1 one could translate the results in Figures 7–10 into errors in real situations.

We also comment on the results for the case with only h_{I} data available, as opposed to the combination of h_{I} and h_{II} data that we used (see § 3.1). In this case, the S/N increase in Figures 5 and 6 is not changed, but the estimation errors are slightly larger ($\sim$30%) than in Figures 7–9 for $M_{Lz} \lesssim 10^7\ M_\odot$ if the errors are normalized to $\mathrm{S/N} = 10^3$. We note that the S/N is $\sqrt{2}$ times smaller than in the case of the two data sets available in Table 1.

TABLE 1

S/N FOR THE VARIOUS BINARY MASSES 10^4–$10^7\ M_\odot$ WITH SOURCE REDSHIFT $z_S = 1, 3, 5, 10$

BINARY MASSES ($M_\odot$)	S/N			
	$z_S = 1$	$z_S = 3$	$z_S = 5$	$z_S = 10$
$10^7 + 10^7$	1038	270	147	66
$10^7 + 10^6$	519	135	74	33
$10^7 + 10^5$	175	46	25	11
$10^7 + 10^4$	52	14	7	3
$10^6 + 10^6$	2575	669	365	164
$10^6 + 10^5$	1517	394	215	97
$10^6 + 10^4$	508	132	72	32
$10^5 + 10^5$	877	228	124	56
$10^5 + 10^4$	310	81	44	20
$10^4 + 10^4$	132	34	19	8

NOTE.—We assume a 1 yr observation of the in-spiral phase before final merging.

5. LENSING EVENT RATE

We discuss the event rate of merging SMBHs and estimate the lensing probability and the lensing event rate. The expected rate of merging SMBHs detected by *LISA* is in the range of 0.1–10^2 events yr^{-1} (Haehnelt 1994, 1998). Recently, Wyithe & Loeb (2003) suggested that some hundreds of detectable events per year could be expected, considering the merger rate at exceedingly high redshift ($z > 5$–10). Thus, we take $\sim$300 events yr^{-1} as the merging event rate.

TABLE 2
LENSING PROBABILITY BY THE LENS MASS IN THE RANGE 10^6–10^9 $M_\odot$ WITH SOURCE REDSHIFT $z_S = 1, 3, 5, 10$

	PROBABILITY			
LENS MODEL	$z_S = 1$	$z_S = 3$	$z_S = 5$	$z_S = 10$
Point-mass lens	<0.21	<1.1	<2.0	<3.9
SIS	7.2×10^{-5}	8.1×10^{-4}	2.0×10^{-3}	4.7×10^{-3}

NOTES.—For the point-mass lens, we give the upper limit that is determined by the observational constraint on the abundance of the compact objects. When the lensing probability is more than 1, the lensing occurs sometimes. For the SIS, CDM halos are assumed to be lenses. The presented values are for the case of $S/N = 10^3$, and hence the results are somewhat overestimated for the binaries of $S/N < 10^3$ in Table 1. If the expected rate of merging SMBHs is $\sim$300 yr^{-1} (Wyithe & Loeb 2003), then the lensing events will be detected at 1 event yr^{-1}.

We consider the lens objects distributed over the universe and calculate the lensing probability for each lens model. For a point-mass lens, we take compact objects (10^6–10^9 $M_\odot$) such as black holes for the lens. Denoting the mass density parameter of compact objects as $\Omega_{\rm co}$, the lensing probability for a source at redshift z_S is (Schneider et al. 1992)

$$P(z_S) = \frac{3}{2}\Omega_{\rm co} y_{\rm cr}^2 \int_0^{z_S} dz_L \, \frac{(1+z_L)^2}{H(z_L)/H_0} \times \frac{H_0 D_{LS}(z_L,\ z_S) H_0 D_L(z_L)}{H_0 D_S(z_S)} , \qquad (35)$$

where $H(z)$ is the Hubble parameter at redshift z. The cosmological abundance of the compact objects in the mass range 10^6–10^9 $M_\odot$ is limited by $\Omega_{\rm co} \leq 0.01$ by the search for multiple images in radio sources (Wilkinson et al. 2001; see also Nemiroff et al. 2001). In Table 2 we show the upper limit on the lensing probability for a point-mass lens. Since we set $y_{\rm cr} = 10$ (eq. [33]), the lensing probability is 100 times larger than that normally assumed for the strong lensing of light ($y_{\rm cr} = 1$). As shown in Table 2, the upper limit of the lensing probability is very high (almost 1) and is typically $\sim(\Omega_{\rm co}/10^{-2})$. The lensing event rate is the product of the merging rate ($\sim$300 yr^{-1}) and the lensing probability, so that the lensing events will be 1 event yr^{-1} if $\Omega_{\rm co} = 10^{-4}$.

For the SIS model we take CDM halos (10^6–10^9 $M_\odot$) as the lens objects (e.g., Narayan & White 1988). The lensing probability is

$$P(z_S) = \pi y_{\rm cr}^2 \int_0^{z_S} dz_L \, \frac{(1+z_L)^2}{H(z_L)/H_0} \frac{H_0 D_{LS}(z_L,\ z_S) H_0 D_L(z_L)}{H_0 D_S(z_S)} \times \int_{10^6\,M_\odot}^{10^9\,M_\odot} dM_L \, v N_v(v,\ z_L) , \qquad (36)$$

where N_v is the comoving number density of the lens and is assumed to be given by the Press-Schechter velocity function (Press & Schechter 1974) with $\sigma_8 = 1$. In Table 2 we show the lensing probability for the SIS model. We set $y_{\rm cr} = 3$ (see Fig. 9), and hence the lensing probability is almost 10 times larger than that for light ($y_{\rm cr} = 1$). As shown in Table 2, the lensing probability is typically $\sim 10^{-4}$ to 10^{-3}. The merger rate is $\sim$300 events yr^{-1} at high redshift ($z > 5$); then, the lensing events would be 1 event yr^{-1}.

We note that the results in Table 2 are for the case of $S/N = 10^3$ and are somewhat overestimated for the binaries of $S/N < 10^3$ in Table 1. For example, the lensing probability is proportional to the S/N from equation (33) for the point-mass lens, and it is appropriate to use $y_{\rm cr} = 1$ for $S/N < 10^3$ in the SIS. In the case of a high event rate ($\sim$300 events yr^{-1}), many fainter signals ($S/N \ll 10^3$) are expected, and we note that the errors in Figures 7–10 are worse for these binaries.

Next, we discuss how we can identify the lensing signal. If a lensing event occurs, the amplitude and the arrival time of the gravitational waves are changed by lensing, but the other features (such as binary mass) are not changed. Thus, if the two signals have the same binary parameters (such as chirp mass) except for the amplitude and the arrival time, that would be a signature of gravitational lensing in the geometrical optics limit. More generally, oscillatory behavior in the waveform $|\tilde{h}^L(f)|$ is a signature of gravitational lensing (see Fig. 4). However, it will be difficult to identify the source and the lens objects in the sky, since the angular resolution of *LISA* is $\sim 1^\circ$ (see Cutler 1998). Furthermore, the gravitational-wave amplitude is changed by the lensing magnification, and hence one must assume the lens model in order to determine the distance to the source. (The effect of lensing on measuring the distance has been recently discussed in Holz & Hughes 2002.) As one determines the distance to the source $D_S(z_S)$, the redshift $z_S(D_S)$ can be determined if the cosmological parameters are well known (see Hughes 2002).

6. SUMMARY

We have discussed the gravitational lensing of gravitational waves from chirping binaries, taking account of the wave effects in gravitational lensing. An SMBH binary is taken as the source detected by *LISA*, and two simple lens models are considered: the point-mass lens and the SIS model. We calculate the lensing effects on the signal-to-noise ratio (S/N) and how accurately the information of the lens object, its mass, can be extracted from the lensed signal. As expected, for a lens mass smaller than 10^8 $M_\odot$, the wave effects are very important in calculating the S/N and the errors in the estimation parameters. It is found for a lens mass smaller than 10^6 $M_\odot$ that the signals are not magnified by lensing because of the diffraction effect. For a lens mass larger than 10^8 $M_\odot$, the lens parameters can be determined within (very roughly) $\sim$0.1% of $[(S/N)/10^3]^{-1}$. We note that the lensing cross section to determine the lens parameters is an order of magnitude larger than that for light.

In this paper, we calculate the case for *LISA*, but a similar analysis can be done for other detectors. For ground-based interferometers (TAMA-300, LIGO, VIRGO, GEO-600), neutron star binaries are taken as the sources, and the lens mass for which wave effects become important is 10–10^4 $M_\odot$. Similarly, for space-based interferometers such as *DECIGO* (Seto et al. 2001), the important lens mass becomes 10^5–10^7 $M_\odot$. Since mergers of neutron star binaries will be detected at at least several per year by LIGO II (Phinney 1991; Kalogera et al. 2001) and $\sim 10^5$ yr^{-1} by *DECIGO*, the lensing events will also be expected for other detectors.

We would like to thank Naoki Seto and Takeshi Chiba for useful comments and discussions. This work was supported in part by Grants-in-Aid 14047212 (T. N.) and 14204024 (T. N.) for Scientific Research of the Japanese Ministry of Education, Culture, Sports, Science, and Technology.

APPENDIX

ESTIMATION ERRORS IN THE GEOMETRICAL OPTICS LIMIT

To evaluate the estimation errors ΔM_{Lz} and Δy in the geometrical optics limit, we consider the simple waveform

$$\tilde{h}^L(f) = \left(|\mu_+|^{1/2} - i|\mu_-|^{1/2} e^{2\pi i f \Delta t_d}\right)\tilde{h}(f) \ , \tag{A1}$$

where $\tilde{h} \propto A$ is the unlensed signal and $\Delta t_d \propto M_{Lz}$, with three parameters $\gamma_i = (\ln M_{Lz},\ y,\ \ln A)$. Then, the Fisher matrix $\Gamma_{ij}(i,\ j = 1,\ 2,\ 3)$ in equation (30) can be analytically obtained as

$$\begin{aligned}
\Gamma_{11} &= \left(2\pi\Delta t_d\right)^2 |\mu_-| \left(f\tilde{h}|f\tilde{h}\right) \ , \\
\Gamma_{12} &= 4\pi^2 \Delta t_d \frac{\partial \Delta t_d}{\partial y} |\mu_-| \left(f\tilde{h}|f\tilde{h}\right) \ , \\
\Gamma_{13} &= 0 \ , \\
\Gamma_{22} &= \frac{1}{4}\left[\frac{1}{|\mu_+|}\left(\frac{\partial|\mu_+|}{\partial y}\right)^2 + \frac{1}{|\mu_-|}\left(\frac{\partial|\mu_-|}{\partial y}\right)^2\right]\left(\tilde{h}|\tilde{h}\right) + \left(2\pi\frac{\partial \Delta t_d}{\partial y}\right)^2 |\mu_-| \left(f\tilde{h}|f\tilde{h}\right) \ , \\
\Gamma_{23} &= \frac{1}{2}\frac{\partial}{\partial y}\left(|\mu_+| + |\mu_-|\right)\left(\tilde{h}|\tilde{h}\right) \ , \\
\Gamma_{33} &= \left(|\mu_+| + |\mu_-|\right)\left(\tilde{h}|\tilde{h}\right) \ ,
\end{aligned} \tag{A2}$$

and $\Gamma_{ji} = \Gamma_{ij}$. In equation (A2) $(\tilde{h}|\tilde{h})$ and $(f\tilde{h}|f\tilde{h})$ are

$$\begin{aligned}
\left(\tilde{h}|\tilde{h}\right) &= (\mathrm{S/N})^2 = 4\int \frac{df}{Sn(f)} \left|\tilde{h}(f)\right|^2 \ , \\
\left(f\tilde{h}|f\tilde{h}\right) &= 4\int \frac{df}{Sn(f)} \left|f\tilde{h}(f)\right|^2 \ .
\end{aligned} \tag{A3}$$

The S/N is for the unlensed signal $\tilde{h}$. The estimation errors can be analytically obtained by the inverse of the Fisher matrix: $\Delta M_{Lz}/M_{Lz} = [(\Gamma^{-1})_{11}]^{1/2}$ and $\Delta y/y = [(\Gamma^{-1})_{22}]^{1/2}/y$. Using the geometrical optics approximation, $f\Delta t_d \gg 1$, we obtain the errors with equations (A2) and (A3) as

$$\begin{aligned}
\frac{\Delta M_{Lz}}{M_{Lz}} &= \frac{1}{\mathrm{S/N}}\sqrt{\frac{|\mu_+| + |\mu_-|}{|\mu_+\mu_-|}}\left|\frac{2(\partial/\partial y)\ln \Delta t_d}{(\partial/\partial y)\ln|\mu_+/\mu_-|}\right| \ , \\
\frac{\Delta y}{y} &= \frac{1}{\mathrm{S/N}}\sqrt{\frac{|\mu_+| + |\mu_-|}{|\mu_+\mu_-|}}\left|\frac{2}{y(\partial/\partial y)\ln|\mu_+/\mu_-|}\right| \ .
\end{aligned} \tag{A4}$$

The above equations (A4) are used for the general lens model when double images form.

REFERENCES

Baraldo, C., Hosoya, A., & Nakamura, T. T. 1999, Phys. Rev. D, 59, 083001
Bender, P. L., et al. 2000, *LISA*: A Cornerstone Mission for the Observation of Gravitational Waves (System & Tech. Study Rep. ESA-SCI 11; Noordwijk: ESA)
Bliokh, P. V., & Minakov, A. A. 1975, Ap&SS, 34, L7
Bontz, R. J., & Haugan, M. P. 1981, Ap&SS, 78, 199
Cutler, C. 1998, Phys. Rev. D, 57, 7089
Cutler, C., & Flanagan, E. F. 1994, Phys. Rev. D, 49, 2658
Cutler, C., & Thorne, K. S. 2002, in Early Universe and Cosmological Observations: A Critical Review, ed. P. Dunsby, G. F. R. Ellis, & R. Maartens (Bristol: IOP), 72
Deguchi, S., & Watson, W. D. 1986a, ApJ, 307, 30
———. 1986b, Phys. Rev. D, 34, 1708
De Paolis, F., et al. 2002, A&A, 394, 749
Finn, L. S. 1992, Phys. Rev. D, 46, 5236
Haehnelt, M. G. 1994, MNRAS, 269, 199
———. 1998, in AIP Conf. Proc. 456, 2d Int. *LISA* Symp. on the Detection and Observation of Gravitational Waves in Space, ed. W. M. Folkner (New York: AIP), 45
Hellings, R. W., & Moore, T. A. 2003, Classical Quantum Gravity, 20, 181
Holz, D. E. & Hughes, S. A. 2002, preprint (astro-ph/0212218)
Hughes, S. A. 2002, MNRAS, 331, 805
Kalogera, V., Narayan, R., Spergel, D. N., & Taylor, J. H. 2001, ApJ, 556, 340
Mandzhos, A. V. 1981, Soviet Astron. Lett., 7, 213
Misner, C. W., Thorne, K. S., & Wheeler, J. A. 1973, Gravitation (San Francisco: Freeman)
Moore, T. A., & Hellings, R. W. 2002, Phys. Rev. D, 65, 062001
Nakamura, T. T. 1998, Phys. Rev. Lett., 80, 1138
Nakamura, T. T., & Deguchi, S. 1999, Prog. Theor. Phys. Suppl., 133, 137
Narayan, R., & White, S. D. M. 1988, MNRAS, 231P, 97
Nemiroff, R. J., et al. 2001, Phys. Rev. Lett., 86, 580
Ohanian, H. C. 1974, Int. J. Theor. Phys., 9, 425
———. 1983, ApJ, 271, 551
Peters, P. C. 1974, Phys. Rev. D, 9, 2207
Peterson, J. B., & Falk, T. 1991, ApJ, 374, L5
Phinney, E. S. 1991, ApJ, 380, L17
Press, W. H., & Schechter, P. 1974, ApJ, 187, 425
Ruffa, A. A. 1999, ApJ, 517, L31
Schneider, P., Ehlers, J., & Falco, E. E. 1992, Gravitational Lenses (New York : Springer)
Schneider, P., & Schmid-Burgk, J. 1985, A&A, 148, 369
Seto, N. 2002, Phys. Rev. D, 66, 122001
Seto, N., Kawamura, S., & Nakamura, T. 2001, Phys. Rev. Lett., 87, 221103
Thorne, K. S. 1983, in Gravitational Radiation, ed. N. Deruelle & T. Piran (Amsterdam: North-Holland), 28
Turner, E. L., Ostriker, J. P., & Gott, J. R. 1984, ApJ, 284, 1
Vecchio, A. 2003, Phys. Rev. D, in press
Vecchio, A., & Cutler, C. 1998, in AIP Conf. Proc. 456, 2d Int. *LISA* Symp. on the Detection and Observation of Gravitational Waves in Space, ed. W. M. Folkner (New York: AIP), 101
Wilkinson, P. N., et al. 2001, Phys. Rev. Lett., 86, 584
Wyithe, J. S. B., & Loeb, A. 2003, ApJ, 590, 691
Zakharov, A. F., & Baryshev, Yu. V. 2002, Classical Quantum Gravity, 19, 1361